



HAL
open science

Adenine Binding Mode Is a Key Factor in Triggering the Early Release of NADH in Coenzyme A-dependent Methylmalonate Semialdehyde Dehydrogenase

Raphael Bchini, H el ene Dubourg-Gerecke, Andr e Aubry, Guy Branlant, Sophie Rahuel-Clermont, Claude Didierjean, Francois Talfournier

► To cite this version:

Raphael Bchini, H el ene Dubourg-Gerecke, Andr e Aubry, Guy Branlant, Sophie Rahuel-Clermont, et al.. Adenine Binding Mode Is a Key Factor in Triggering the Early Release of NADH in Coenzyme A-dependent Methylmalonate Semialdehyde Dehydrogenase. *Journal of Biological Chemistry*, 2012, 287 (37), pp.31095-31103. 10.1074/jbc.M112.350272 . hal-01682573

HAL Id: hal-01682573

<https://hal.univ-lorraine.fr/hal-01682573>

Submitted on 12 Jan 2018

HAL is a multi-disciplinary open access archive for the deposit and dissemination of scientific research documents, whether they are published or not. The documents may come from teaching and research institutions in France or abroad, or from public or private research centers.

L'archive ouverte pluridisciplinaire **HAL**, est destin ee au d ep ot et  a la diffusion de documents scientifiques de niveau recherche, publi es ou non,  emanant des  tablissements d'enseignement et de recherche fran ais ou  trangers, des laboratoires publics ou priv es.

Adenine Binding Mode Is a Key Factor in Triggering the Early Release of NADH in Coenzyme A-dependent Methylmalonate Semialdehyde Dehydrogenase^{*[5]}

Received for publication, February 7, 2012, and in revised form, July 2, 2012. Published, JBC Papers in Press, July 10, 2012, DOI 10.1074/jbc.M112.350272

Raphaël Bchini^{†1}, Hélène Dubourg-Gerecke^{§1}, Sophie Rahuel-Clermont[‡], André Aubry^{§†}, Guy Branlant^{†‡2}, Claude Didierjean[§], and François Talfournier^{†‡3}

From the [†]Unité Mixte de Recherche CNRS-Université de Lorraine 7214 AREMS, ARN-RNP Structure-Fonction-Maturation, Enzymologie Moléculaire et Structurale, Faculté de Médecine, Biopôle, 9 Avenue de la Forêt de Haye, BP 184, 54506 Vandœuvre-lès-Nancy, France and the [§]Unité Mixte de Recherche Cristallographie, Résonance Magnétique et Modélisations, Equipe Biocristallographie, UMR 7036 CNRS-Université de Lorraine, Faculté des Sciences et Technologies, BP 70239, 54506 Vandœuvre-lès-Nancy Cedex, France

Background: Conformational dynamics of the cofactor are essential for catalysis by hydrolytic ALDHs.

Results: Crystallographic and kinetic data reveal the molecular basis for NADH release in MSDH, a CoA-dependent ALDH.

Conclusion: Weaker stabilization of the adenine ring triggers early NADH release in MSDH-catalyzed reaction.

Significance: First description of the mechanism whereby the cofactor binding mode is partly responsible for the kinetic behavior of CoA-dependent ALDHs.

Structural dynamics associated with cofactor binding have been shown to play key roles in the catalytic mechanism of hydrolytic NAD(P)-dependent aldehyde dehydrogenases (ALDH). By contrast, no information is available for their CoA-dependent counterparts. We present here the first crystal structure of a CoA-dependent ALDH. The structure of the methylmalonate semialdehyde dehydrogenase (MSDH) from *Bacillus subtilis* in binary complex with NAD⁺ shows that, in contrast to what is observed for hydrolytic ALDHs, the nicotinamide ring is well defined in the electron density due to direct and H₂O-mediated hydrogen bonds with the carboxamide. The structure also reveals that a conformational isomerization of the NMNH is possible in MSDH, as shown for hydrolytic ALDHs. Finally, the adenine ring is substantially more solvent-exposed, a result that could be explained by the presence of a Val residue at position 229 in helix α_F that reduces the depth of the binding pocket and the absence of Gly-225 at the N-terminal end of helix α_F . Substitution of glycine for Val-229 and/or insertion of a glycine residue at position 225 resulted in a significant decrease of the rate constant associated with the dissociation of NADH from the NADH/thioacylenzyme complex, thus demonstrating that the weaker stabilization of the adenine ring is a key factor in triggering the early NADH release in the MSDH-catalyzed reaction. This study provides for the first time structural insights

into the mechanism whereby the cofactor binding mode is responsible at least in part for the different kinetic behaviors of the hydrolytic and CoA-dependent ALDHs.

Among the many enzymes that metabolize aldehydes, the members of the aldehyde dehydrogenase (ALDH)⁴ superfamily play a critical role in protecting cells against the cytotoxic and carcinogenic effects of aldehydic compounds. In humans, the clinical importance of ALDHs is supported by the fact that mutations and polymorphisms in ALDH genes that lead to defective aldehyde metabolism are the molecular basis of severe diseases (1, 2). Moreover, several ALDHs appear to be markers for normal and cancer stem cells (3, 4). ALDHs are also known to play central roles in many essential biological functions such as intermediary metabolism, embryogenesis, development, and neurotransmission.

The ALDHs catalyze the NAD(P)⁺-dependent oxidation of a wide variety of aldehydes to their corresponding non-activated or CoA-activated acids via a common two-step chemical mechanism. The acylation step involves the formation of a hemithioacetal intermediate via the nucleophilic attack of the catalytic Cys-302 (the amino acid numbering used for the biochemical and structural data is that defined by Wang and Weiner (5)) on the aldehydic function followed by hydride transfer that leads to formation of a thioacylenzyme intermediate and NAD(P)H. This intermediate then undergoes a nucleophilic attack by an activated water or CoA molecule. Over the past 15 years both mechanistic and structural aspects of hydrolytic ALDHs have been studied extensively (5–13). In addition to local conformational reorganizations of the active site induced by ligand binding that provide the required flexibility

* This work was supported in part by the CNRS, the University of Nancy I, the Institut Fédératif de Recherche 111 Bioingénierie, and local funds from the Région Lorraine.

[5] This article contains supplemental Figs. S1–S6.

The atomic coordinates and structure factors (code 1T90) have been deposited in the Protein Data Bank, Research Collaboratory for Structural Bioinformatics, Rutgers University, New Brunswick, NJ (<http://www.rcsb.org/>).

[†] Deceased.

¹ Both authors contributed equally to this work and were supported by the French Research Ministry.

² To whom correspondence may be addressed. E-mail: guy.branlant@maem.uhp-nancy.fr.

³ To whom correspondence may be addressed. E-mail: francois.talfournier@maem.uhp-nancy.fr.

⁴ The abbreviations used are: ALDH, aldehyde dehydrogenase; ALDH2, class 2 ALDH; MMSA, methylmalonate semialdehyde; MSDH, methylmalonate semialdehyde dehydrogenase; RALDH2, retinal dehydrogenase 2.

Cofactor Dynamics in ALDH Superfamily

for an efficient catalysis (14, 15), one of the key aspects of the chemical mechanism of this ALDH family is the substantial conformational flexibility of the NMN moiety of the cofactor and in particular of the nicotinamide ring.⁵ Indeed, the presence of multiple conformations of the NMN moiety is supported by the majority of the x-ray structures of ALDH-NAD(P)⁺ binary complexes as well as NMR studies and has been hypothesized to be due to the peculiar binding mode of the cofactor to a non-canonical Rossmann fold (9, 16–18). Furthermore, significant efforts have been made to characterize the mode by which the cofactor is stabilized during both the acylation and the deacylation steps. In the acylation step, the NMN moiety must be positioned such that an efficient and stereospecific hydride transfer can occur from the hemithioacetal intermediate to the C-4 of the nicotinamide. The side chain of invariant Glu-399 was shown to play an essential role in this stabilization by anchoring the NMN ribose through hydrogen bonds with its hydroxyl groups (19). Moreover, recent studies support a critical contribution of the β -methyl group of the invariant Thr-244 residue that allows the nicotinamide ring to adopt a productive conformation for hydride transfer (20). Nevertheless, this conformation is not suitable for the deacylation because it would sterically preclude the catalytic Glu-268 from playing its role in the hydrolytic process. The fact that the cofactor remains bound to the enzyme along the two-step catalytic mechanism strongly suggested that movement of the reduced NMN (NMNH) moiety of the NAD(P)H is a prerequisite for completion of the second half of the reaction (21). Indeed, the first structural evidence for this conformational change of the NMNH during the catalytic cycle of hydrolytic ALDHs was provided by the crystal structure of a thioacyl-enzyme intermediate-NADPH complex (7). Specifically, this structure revealed that once the acylation step has occurred, the reduced cofactor adopts a new conformation with a flip of the NMNH moiety, which positions the reduced nicotinamide in a conserved cavity that might constitute the exit door for NAD(P)H.

By contrast, less information is available concerning structural and/or mechanistic aspects of the CoA-dependent ALDHs. In an effort to address this gap in knowledge, our group has for several years been studying the catalytic mechanism of the methylmalonate semialdehyde dehydrogenase (MSDH) from *Bacillus subtilis* (22, 23). This homotetrameric enzyme catalyzes the NAD⁺-dependent oxidation of methylmalonate semialdehyde (MMSA) and malonate semialdehyde to propionyl- and acetyl-CoA, respectively, and has been reported to be involved in *myo*-inositol catabolism (24). In mammals, MSDH is a mitochondrial enzyme that participates in the distal portions of the valine and pyrimidine catabolic pathways (25). A possible correlation between organic acidemia and MSDH deficiency has been explored (26, 27), and very recently, Sass *et al.*

(28) proposed that polymorphism in the human *ALDH6A1* gene encoding MSDH is directly correlated with 3-hydroxybutyric aciduria, a severe metabolic disease. Detailed kinetic studies of the MSDH-catalyzed reaction have shown that (i) the rate constant associated with the acylation step is high ($k_{ac} > 1000 \text{ s}^{-1}$), indicating that the position of the nicotinamide ring relative to the hemithioacetal allows efficient hydride transfer, and (ii) that NADH release occurs before the rate-limiting β -decarboxylation and CoA attack on the thioacyl-enzyme intermediate (22), thus supporting the ping-pong kinetic mechanism that has previously been reported for other CoA-dependent ALDHs (29, 30).

Taken together these data raise important questions regarding the evolution of the catalytic mechanism within the ALDH superfamily. In particular, it is of interest to determine whether the pattern of interactions that is thought to stabilize an efficient hydride transfer conformation of the NMN moiety of the cofactor in the hydrolytic ALDHs is also operative in the members of the CoA-dependent family. Additionally, two key aspects related to the structural dynamics associated with the release of the reduced cofactor remain to be addressed, (i) whether cofactor isomerization after hydride transfer occurs in CoA-dependent ALDHs and ii) the molecular and structural factors responsible for the early or late release of the reduced cofactor occurring in the catalytic cycle of CoA-dependent and hydrolytic ALDHs, respectively.

We detail here the first crystal structure of a CoA-dependent ALDH. The structure of the binary MSDH/NAD⁺ complex shows that, in contrast to what is observed in nearly all x-ray structures of hydrolytic ALDH-NAD(P)⁺ binary complexes, the nicotinamide ring is well defined in the electron density due to direct and H₂O-mediated hydrogen bonds between the amino group of the carboxamide and residues belonging to the cofactor binding and the catalytic domains. Moreover, the pocket that is postulated to constitute the exit door of the reduced cofactor in the hydrolytic ALDHs is conserved, thus suggesting that a cofactor isomerization also occurs in MSDH and the entire CoA-dependent ALDH family. Finally, superimposition of all ALDH holo-structures reveals that the adenine ring of NAD⁺ is substantially more solvent-exposed in MSDH. Analysis of the adenine binding pocket highlights several structural factors that could explain this marked difference; (i) the presence of a Val residue at position 229 in the MSDH that reduces the depth of the binding pocket, thereby increasing the solvent exposure of the adenine ring, and (ii) the absence of Gly-225 at the N-terminal end of helix α_F . These observations suggest a major role for the adenine binding mode in the dynamics of the reduced cofactor in the MSDH catalytic mechanism. Indeed, substitution of glycine for Val-229 and/or insertion of a glycine residue at position 225 in the MSDH from *B. subtilis* resulted in a significant decrease of the rate constant associated with the dissociation of NADH from the NADH/thioacyl-enzyme complex, thus validating this assumption.

EXPERIMENTAL PROCEDURES

Materials—NAD⁺ was purchased from Roche Applied Science. CoA, pyruvate, and lactate dehydrogenase (LDH) were from Sigma. MMSA was synthesized as described by Kupiecki

⁵ The nicotinamide ring is well defined in the electron density maps in the crystal structures of η -crystallin (PDB code 1o9j) and ALDH1L1 (PDB code 2O2Q). However, η -crystallin is an inactive ALDH that acts as a UV/blue light filter in the lens, whereas in ALDH1L1 the stabilization of the nicotinamide ring is mainly achieved by formation of a covalent adduct between the C4 of the ring and the catalytic cysteine that is likely non-catalytically relevant.

and Coon (31), and its concentration was determined by titration with MSDH.

Site-directed Mutagenesis, Production, and Purification of Wild-type and Mutated MSDHs from *B. subtilis*—Site-directed mutagenesis was performed using standard PCR site-directed mutagenesis. Wild-type and mutated MSDHs were produced and purified using a procedure described previously (22). Enzyme concentrations were determined spectrophotometrically by using molar absorption coefficients of $2.04 \times 10^5 \text{ M}^{-1} \cdot \text{cm}^{-1}$ at 280 nm for wild-type and mutated MSDHs. In the present paper, enzyme concentrations are expressed per monomer (normality, N).

Kinetic Parameters for Wild-type and Mutated MSDHs under Steady-state Conditions—Initial rate measurements were carried out at 30 °C on a SAFAS UV mc2 spectrophotometer by following the appearance of NADH at 340 nm in 50 mM potassium phosphate (pH 8.2). Before kinetic measurements in the presence of MMSA, wild-type and mutated MSDHs were preincubated at 30 °C with 2 mM NAD^+ to activate the enzyme and eliminate the lag-phase exhibited by progress curves for enzymatic turnover (22). The initial rate data were fit to the Michaelis-Menten equation using nonlinear least-squares regression analysis to determine the k_{cat} and K_m values. All K_m values were determined at saturating concentrations of the other substrates.

Pre-steady-state Kinetic Measurements—Pre-steady-state kinetic analyses were carried out on a SX18MV-R stopped-flow apparatus (Applied PhotoPhysics), and collected data were analyzed using the SX18MV-R software package.

Kinetics of the Acylation Step and of NADH Dissociation of Mutated MSDHs—To study the acylation step, progress curves of NADH production were recorded at 340 nm and at 30 °C in 50 mM potassium phosphate (pH 8.2) in the absence of CoA. One syringe was filled with 32 μM MSDH and 2 mM NAD^+ , and the other contained 2 mM MMSA.

To evaluate the rate of NADH dissociation from the thioacylenzyme-NADH complex, the coupled pyruvate/lactate dehydrogenase (LDH) assay was used as an NADH trapping system. One syringe was filled with 32 μM MSDH and 2 mM NAD^+ , and the other contained 1 mM MMSA, 32 μM LDH, and 20 mM pyruvate. Experiments were carried out in the absence of CoA in 50 mM potassium phosphate (pH 8.2) at 30 °C. Data were fit to a biphasic expression.

Crystallization, Data Collection, and Processing—Orthorhombic crystals of the MSDH from *B. subtilis* were obtained from a concentrated protein solution (200 mg/ml) and in the presence of 10 mM NAD^+ . Ammonium sulfate was used as precipitant agent. Detailed protocols for MSDH expression, purification, crystallization, and preliminary x-ray analysis were reported previously (32).

Phasing and Refinement—The structure of the MSDH from *B. subtilis* was solved by molecular replacement, revealing that MSDH crystallizes with one homotetramer per asymmetric unit like the cod liver betaine aldehyde dehydrogenase used as a search model (18) (PDB entry 1bpw). The structure was initially refined using rigid body minimization and simulated annealing procedures before iterative cycles of manual rebuilding and refinement. Using 20–2.5 Å data, the final R_{free} and R_{cryst} values

TABLE 1
Statistics of x-ray diffraction data collection and model refinement
Values in parentheses refer to the outermost resolution shell.

Space group	$P2_12_12_1^a$
Unit-cell parameters (Å)	$a = 195.2, b = 192.5, c = 83.5^a$
Resolution range (Å)	20.0–2.5 ^a (2.50–2.59)
R_{merge} (%)	13.8 (37.2) ^a
$\langle I/\sigma(I) \rangle$	9.4 (3.6) ^a
Completeness	99.5 (91.5)
Redundancy	7.3
Refinement	
Resolution range (Å)	20.0–2.5
No. of reflections	108,345 ^a
R/R_{free} (%)	21.1/25.0
No. of atoms	
Protein	3742 per monomer (A, B, C, D)
Ligand (NAD)	44 in each monomer
Water	866
B-factors (Å ²)	
Protein	29.7
Ligand (NAD)	42.0
Water	28.5
Ramachandran statistics (%)	
Residues in preferred regions	89.8
Residues in allowed regions	9.3
Outlier residues	0.9
Root mean square deviations	
Bond lengths (Å)	0.006
Bond angles (°)	1.3

^a From Ref. 32.

were 0.25 and 0.211, respectively. The asymmetric unit consisted of 4 polypeptide chains (in all monomers, residues Glu-3–Phe-486), 4 NAD^+ molecules, and 866 water molecules. The first two residues and the last residue were not found in electron density maps and so are presumably disordered. The MSDH structure exhibited good geometry, with 89.9% of all residues in the most favored and 9.3% in the allowed regions of the Ramachandran plot as indicated by the program Procheck (33). Molecular replacement calculations and structure refinement were carried out using the CNS program package (34). The graphics programs TurboFrodo (35) and PyMOL were used in model building and in preparation of figures, respectively. Further statistics are summarized in Table 1. The refined coordinates of the model of MSDH and the structure factors have been deposited with the Protein Data Bank under accession code 1T90.

RESULTS AND DISCUSSION

Overall Structure—As expected, the three-dimensional structure of the MSDH from *B. subtilis* conforms to known tetrameric ALDH structures; the tetramer of the enzyme is a dimer of dimers with strong interactions at the dimer interface but weaker interactions at the tetramer interface (11), and the monomer consists of three domains, the dinucleotide binding domain (residues 3–123 and 141–251), the catalytic domain (residues 252–270), and a small domain (residues 124–140 and 471–486) involved in the oligomerization (Fig. 1). A structural comparison with available entries in the Protein Data Bank database was performed using the PDBeFold server (36). The root mean square deviations upon comparing the C α traces of all available monomer structures vary from 1.4 to 2.5 Å, the most similar and distant structures being that of betaine aldehyde dehydrogenase from *Pseudomonas aeruginosa* (PDB code 2wme (37)) and that of dimeric ALDH3 (PDB code 1ad3 (9)).

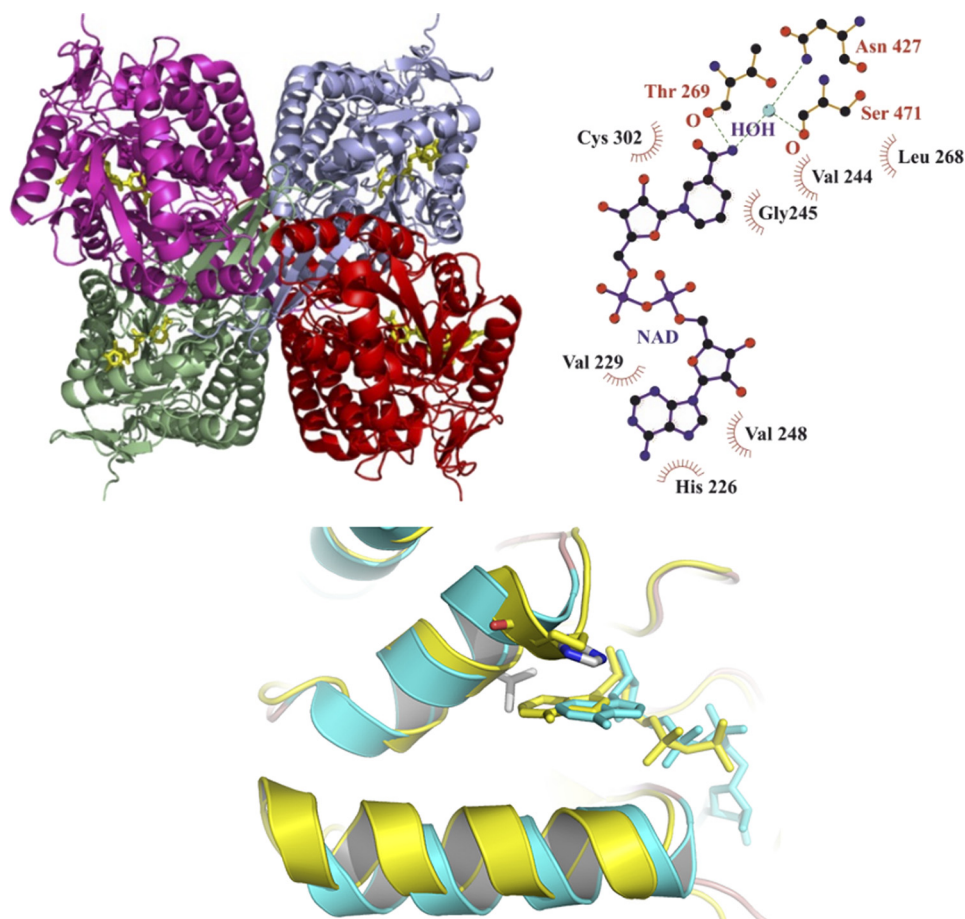


FIGURE 1. **Schematic drawings of the crystal structure of *B. subtilis* MSDH.** Upper left, schematic representation of the overall fold of the MSDH tetramer in which the individual subunits are colored differently. NAD molecules are shown as yellow sticks. Upper right, LIGPLOT drawing (41) of the MSDH NAD binding site. The residues involved in the stabilization of the ribose and pyrophosphate moieties are omitted for clarity. Down, superimposition of schematic representation of the adenine binding site of MSDH (blue) and rat RALDH2 (yellow) is shown. Residues at positions 226 and 229 are represented as sticks colored by atom type and yellow for MSDH and rat RALDH2, respectively. NAD molecules are represented as sticks colored according to the corresponding binding pocket.

The crystal structure of the MSDH from *B. subtilis* did not reveal significant structural differences between the four monomers within each asymmetric unit. Indeed, the average root mean square deviation value obtained from the different pairwise superimpositions of the $C\alpha$ atoms was 0.23 Å, and the monomers exhibited similar average isotropic displacement parameters. Each monomer is occupied by a NAD^+ molecule that is well defined in the final $2|F_o| - |F_c|$ electron density map (supplemental Fig. S1).

Catalytic Site—Irrespective of the monomer, the side-chain orientation of Cys-302 is similar to that depicted to be catalytically competent for hydrolytic ALDHs (21). At first sight, this observation contradicts our previous data because NAD^+ binding was shown to elicit a slow conformational change that likely provokes a reorientation of only two Cys-302 residues per tetramer and also a local rearrangement within the dimer interface. Moreover, the presence of two populations of Cys-302 correlated well with the half-site reactivity exhibited by the enzyme (*i.e.* only two subunits are active per tetramer). The apparent discrepancy between solid state and solution data may be explained by either the average crystallographic resolution of the structure or by the much longer time scales for crystallization assays relative to the kinetic experiments. The latter hypothesis is further supported by the low resolution (2.9 Å)

x-ray structure of a thioacylenzyme intermediate recently obtained by soaking the crystals of the binary MSDH/ NAD^+ complex with MMSA, which revealed that in each monomer the catalytic Cys-302 exhibits an additional electron density consistent with the presence of a covalently linked substrate molecule (data not shown). Therefore, the quasi-perfect 222 symmetry of the MSDH structure is not helpful in revealing the molecular basis for the half-site reactivity exhibited by the enzyme. In particular, a critical role of a coenzyme-induced disorder-to-order transition of the loop located at the dimer interface, *i.e.* connecting β_{18} and α_N (supplemental Fig. S2), as proposed for the human ALDH2, remains to be validated (38).

The nicotinamide ring of NAD^+ is well defined in the electron density maps and is sandwiched between the catalytic Cys-302 on the A-side and the Val-244 and Gly-245 residues on the B-side, respectively. The short distance (3.15 Å) between the sulfur atom of Cys-302 and the C4 atom of the nicotinamide suggests that the NMN portion adopts the so-called “hydride transfer” conformation (21). In addition, the thiol of Cys-302 is positioned between the amide groups of Asn-169 and Asn-427. Asn-169 is invariant within the ALDH superfamily, and its amide group as well as the main-chain nitrogen of Cys-302 were shown to make up an oxyanion hole that allows for an efficient hydride transfer without assistance by a base-catalyst (6). By

contrast, Asn-427 is MSDH-specific and is replaced by Leu in the hydrolytic family (see below and supplemental Fig. S2).

The substrate access tunnel of MSDH can be divided in two parts: a narrow region surrounding the catalytic Cys-302 and a wide region near the tetramer interface. The narrow region can be described as a hydrophobic crown comprising the side chains of Phe-170, Met-173, Trp-177, Met-303, Ala-459, Phe-465, and the aliphatic portion of Arg-301. These seven residues are strictly conserved in the MSDH family except for Ala-459, which is located in the long loop referred to as the substrate specificity loop by Moore *et al.* (39). Nevertheless, the hydrophobic character of the position 459 is conserved as only Ala and Val are found in known MSDH sequences. The entrance of the narrow part of the catalytic tunnel comprises, notably, the side chains of Arg-124 and Arg-301. Very recently, both residues were shown to participate not only in MMSA binding through stabilizing electrostatic interactions with the carboxylate group of the substrate but likely also in positioning MMSA efficiently relative to Cys-302 in the MSDH/NAD⁺/MMSA ternary complex (23).

NMN Binding Site—The four NAD⁺ binding sites are occupied by a cofactor molecule and appear to be equivalent as the four NAD⁺ mean B factors are quite similar (41.2, 42.9, 43.1 and 42.5 Å²). As mentioned above, each dinucleotide molecule is well defined in the electron density map and adopts the extended conformation reported to be suitable for efficient hydride transfer. When compared with other known tetrameric structures of hydrolytic ALDHs, the greatest structural differences are observed in the nicotinamide and adenine binding pockets. First, the MSDH structure reveals a major difference in the stabilization mode of the nicotinamide ring that is well defined in the electron density maps, in contrast to what has been observed in nearly all x-ray structures of binary ALDH-NAD(P)⁺ complexes.⁵ This difference could originate from a stabilization of its conformation through hydrogen bonds between the carboxamide group and the carbonyl group of Thr-269 on the one hand and a water molecule held in position by the carbonyl group of Ser-471 and the side chain of Asn-427 on the other hand (Fig. 1). We, therefore, generated the N427L substitution to determine the consequence of the loss of this MSDH-specific hydrogen bond. This substitution dramatically altered the catalytic properties of the enzyme. The acylation became rate-limiting with a decrease of the associated rate constant by at least 10⁵-fold relative to the wild-type MSDH (*i.e.* <10⁻² versus > 1000 s⁻¹). Although it was not possible to determine whether hydride transfer was rate-determining within the acylation step because of the very low *k*_{cat} value, the dramatic decrease of the *k*_{cat} is likely the consequence of the disruption of the H₂O-mediated hydrogen bond interaction between the carboxamide and the Asn-427, thus leading to formation of an inefficient N427L ternary complex.

By contrast, several interactions known to be essential in the hydrolytic ALDHs for maintaining a productive conformation of the NMN moiety are conserved. The NMN ribose remains anchored through hydrogen bonds between its hydroxyl groups and the side chain of the invariant Glu-399. Additionally, one of the two methyl groups of the β-branched side chain of Val-244 is positioned similarly to the β-methyl of invariant Thr-244 in

hydrolytic ALDHs. Therefore, the methyl could fulfill a similar function as that of Thr-244 due to its positioning via the hydrophobic interaction of the second β-methyl with the side chain of Met-178. Altogether, these structural data suggest that the “classical” pattern of interactions proposed to participate in the stabilization of an efficient hydride transfer conformation of the NMN moiety of the cofactor, once the transient hemithioacetal intermediate is formed, is also operative in the MSDH, a result that is likely generalizable to CoA-dependent ALDHs. However, the contribution of Val-244 in stabilizing the nicotinamide conformation appears not sufficient, whereas the carboxamide/Asn-427 interaction is shown to be essential.

Interestingly, the pocket that is postulated to constitute the exit door of the reduced cofactor in the hydrolytic ALDHs (supplemental Fig. S3) and the interaction pattern that enables the pyrophosphate group to be pliable are conserved (data not shown). Therefore, a conformational isomerization of the NMNH is possible, but questions remain concerning its mechanistic relevance. In accordance with the ping-pong kinetic mechanism, NADH release occurs before the transthioesterification step. This rules out the requirement for a flip of the NMNH for CoA binding, an assertion that is further supported by our recent kinetic data showing that the NAD(H) and CoA binding sites do not overlap (23). An alternative explanation is that nucleophilic attack of the CoA on the decarboxylated thioacylenzyme intermediate is not possible if NMNH is present in the active site due to potential steric hindrance. Nevertheless, this hypothesis requires additional structural data to be validated, in particular characterization of the CoA binding site. As the putative structural dynamics associated with the NMN(H) moiety did not provide any clues as to the molecular basis responsible for the early release of the reduced cofactor in the catalytic mechanism of the MSDH, we investigated the possibility that this difference could originate from significant disparities in the adenosine binding mode.

Adenosine Binding Site—Superimposition of all available ALDH holo-structures revealed that the adenine ring is substantially more solvent-exposed in MSDH (Fig. 1). Analysis of the adenine binding pocket highlighted several structural factors that could explain this marked difference. The adenine ring fits between the N-terminal parts of the α_F and α_G helices, making van der Waals contacts with the side chains of His-226 and Val-229 from α_F and of Val-249 from α_G, respectively (supplemental Fig. S4A). The Val-249 residue is well conserved in all ALDHs including MSDHs, but His-226 and Val-229 are MSDH-specific (supplemental Figs. S2 and S5). The presence of invariant Val-229 in MSDH reduces the depth of the binding pocket, thereby increasing the solvent exposure of the adenine ring. In hydrolytic ALDHs, this residue is replaced by a glycine or an alanine, whereas the residue corresponding to His-226 is quite variable (except for eukaryotes where a proline is preferentially observed) (supplemental Fig. S2). In addition, the residue corresponding to Gly-225 is also missing, an invariant feature in MSDH sequences (supplemental Fig. S5). It was thus tempting to postulate that the adenine binding mode plays a key role in the dynamics of the reduced cofactor during the MSDH catalytic cycle. To validate this assumption, we first attempted to improve the stabilization of the adenine ring through substi-

TABLE 2

Kinetic parameters of the reactions catalyzed by wild-type and mutated MSDHs under steady-state conditions

Kinetic parameters were deduced from nonlinear regression of experimental data sets according to the Michaelis-Menten equation. All K_m values were determined at saturating concentrations of the other substrates, and k_{cat} values are expressed per active subunit (*i.e.* two active subunits per tetramer). The steady-state initial rates of the reaction of mutated MSDHs were measured at 30 °C in 50 mM potassium phosphate buffer (pH 8.2) under similar conditions as those for the wild-type MSDH. Mutated MSDHs were preincubated with 2 mM NAD at 30 °C before making the kinetic measurements.

	K_m			k_{cat} s^{-1}	Rate-limiting step
	NAD ⁺	MMSA	CoA		
Wild type	2.3 ± 0.1 mM	60 ± 10 μM	120 ± 20 μM	2.2 ± 0.2	Deacylation
V229G	0.57 ± 0.08	54 ± 7	234 ± 30	0.78 ± 0.03	Deacylation
::G225	0.69 ± 0.05	22 ± 4	151 ± 18	0.39 ± 0.01	Deacylation
V229G/::G225	0.15 ± 0.02	27 ± 4	63 ± 4	0.21 ± 0.01	Deacylation
V229G/H226P	0.66 ± 0.19	28 ± 6	119 ± 25	0.090 ± 0.007	Acylation
V229G/::G225/H226P	0.77 ± 0.10	21 ± 5	96 ± 23	0.020 ± 0.006	Acylation
V229G/::G225/Y252L/ V253I	9.44 ± 1.12	215 ± 43	497 ± 126	0.020 ± 0.007	Acylation

^a Data are from Ref. 22.

tution of glycine for Val-229 and insertion of glycine at position 225 (::G225). If our hypothesis was correct, we expected to observe a significant decrease in the rate constant (k_{off}) associated with the dissociation of NADH from the thioacylzyme/NADH complex relative to wild-type MSDH.

For the wild-type MSDH-catalyzed reaction, the rate-limiting step was shown to be associated with β -decarboxylation within the deacylation step. It was also demonstrated that the β -decarboxylation of the thioacylzyme intermediate occurs after NADH release and before transthioesterification (22). Therefore, before interpreting the steady-state kinetic data and the k_{off} values, it was necessary to establish whether the rate-limiting step was still associated with deacylation for the mutated MSDHs. Accordingly, fast kinetic experiments were carried out for all mutated MSDHs at 30 °C and pH 8.2 in the presence of saturating concentrations of NAD⁺ and MMSA under presteady-state conditions (*i.e.* in the absence of CoA).

Kinetic Properties of Mutated V229G, ::G225 and V229G/::G225 MSDHs—A burst magnitude of 2 mol of NADH/mol of tetramer was observed irrespective of the mutated MSDHs. These data indicate that all mutated MSDHs also exhibited half-site reactivity, as described for the wild type. More importantly, the k_{obs} values of 152, 94, and 173 s⁻¹ were 195-, 241-, and 824-fold higher than the k_{cat} values for the V229G, ::G225 and V229G/::G225 MSDHs, respectively. This result shows that the rate-limiting step still takes place after hydride transfer. Its efficiency remains high but is significantly decreased, as the k_{obs} values are 7- to 13-fold lower relative to wild-type MSDH. This drop in rate constant could be the consequence of minor changes occurring in the location and orientation of the nicotinamide relative to the hemithioacetal intermediate within the mutated ternary complexes, thereby slowing down hydride transfer. One possible explanation is that modifications in the adenine binding pocket initiated a cascade of structural changes that disturbed the nicotinamide positioning within the covalent ternary complex. Interestingly, this hypothesis is supported by the recent work of Tsybovsky and Krupenko (40), who proposed that long-range communication between the active site and the cofactor binding domain in ALDH1L1, involving an α -helix (α_G) that forms one-half of the adenine binding pocket, partly controls the binding of the cofactor.

The kinetic parameters determined at pH 8.2 and 30 °C under steady-state conditions are summarized in Table 2.

Whereas the K_m values determined for MMSA and CoA were not significantly modified, the k_{cat} and K_m values for NAD⁺ decreased from 2.8- to 10.5-fold and from 3- to 15-fold for mutated MSDHs, respectively. However, it is not possible to interpret with confidence the significance of the decrease in K_m for NAD observed for mutated MSDHs as the K_m cannot be equated with the dissociation constant of the enzyme-substrate complex(es).

As previously mentioned, the rate-limiting step still occurs after hydride transfer. It was thus possible to evaluate the consequence(s) of the mutations introduced in the adenine pocket on the rate constant of NADH dissociation from the thioacylzyme-NADH complex through the use of LDH as an NADH-trapping system. The experiments were performed at pH 8.2 and 30 °C under presteady-state conditions in the absence of CoA. The resulting progress curves were fit to a biphasic expression; the first kinetic phase represents the burst of NADH production associated with the acylation process, whereas the second corresponds to the titration by LDH of NADH that dissociates from the thioacylzyme-NADH complex. Under the experimental conditions used, the rate constant associated with the NADH oxidation by LDH (130 s⁻¹) is higher than the apparent rate constants (k_{off}) of 2.7, 1, and 1 s⁻¹, which can be assigned to release of NADH from the thioacylzyme-NADH complex for the V229G, ::G225 and V229G/::G225 MSDHs, respectively (Fig. 2). This result shows that NADH release still occurs before CoA adds, as for the wild-type MSDH (22). This is further supported by additional experiments done in the presence of Desulfo-CoA which show that for V229G/::G225 MSDH, the binding of this inactive analog impedes NADH release (supplemental Fig. S6). This conclusion can reasonably be extended to V229G and ::G225 MSDHs. The fact that the k_{off} are 20- and 56-fold lower than that determined for wild-type MSDH (56 s⁻¹ (22)) provides strong experimental support for a key role of the adenine binding mode in the dynamics of the reduced cofactor in the MSDH catalytic pathway.

For V229G MSDH, the 20-fold decrease in k_{off} for NADH likely reflects a movement of the adenine ring into the void created by the absence of steric hindrance at position 229; this relocation allows for a significant improvement in adenine stabilization through additional contacts within the binding pocket. The explanation is different for ::G225 MSDH because

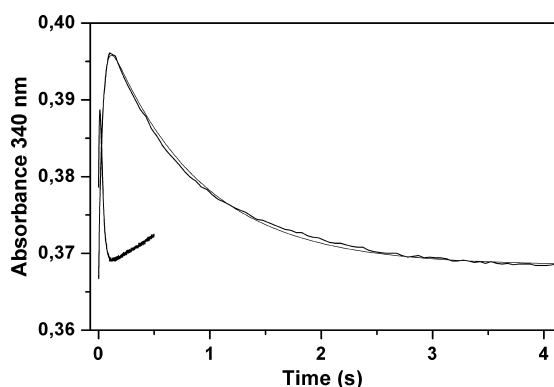


FIGURE 2. Representative transient for the determination of the NADH dissociation rate from the V229G::G225 thioacylenzyme intermediate. A solution of 32 μM "activated"-MSDH, 32 μM LDH (expressed in subunit), and 20 mM pyruvate was rapidly mixed at 30 °C with an equal volume of 2 mM NAD^+ and 0.5 mM MMSA (final concentrations). Both syringes contained 50 mM potassium phosphate buffer (pH 8.2). Under the same experimental conditions, the rate of oxidation of free NADH by LDH was shown to be 130 s^{-1} . The collected data were fit to a triphasic or biphasic expression for the wild-type (thick line, (22)) and V229G::G225 (thin line) MSDHs, respectively. The first phase represents the acylation step, and the second phase represents the consumption of NADH after its release from the thioacylenzyme-NADH complex, whereas the third phase observed for the wild-type MSDH is likely due to the reverse LDH-catalyzed reaction. For the V229G::G225 MSDH, the rate constants obtained for the global fitting are 29 ± 1 and $1.0 \pm 0.1 \text{ s}^{-1}$, respectively. The burst of NADH appears smaller for the wild-type enzyme because the rate constants associated with the two phases are very similar (72 versus 56 s^{-1}) compared with those determined for the mutated MSDH.

this insertion instead increased the length of the loop located at the N-terminal end of the α_{F} helix. Thus, it is reasonable to postulate that the 56-fold decrease in k_{off} for NADH results from a conformational change(s) of this loop that might provide a supplemental anchor point(s) that improves the stabilization of the adenine ring. However, although each single mutation led to significant kinetic effects, they were not additive, as no additional decrease in k_{off} was observed for the double mutant. Finally, the fact that the k_{off} values are only 2.5- to 5-fold higher than the k_{cat} values shows that β -decarboxylation likely remains rate-limiting irrespective of the mutated MSDHs. Nonetheless, the decrease in k_{cat} compared with the wild-type MSDH is mainly the consequence of the significant decrease in the k_{off} values. Therefore, NADH release can be considered to be partially rate-limiting.

Kinetic Properties of Mutated V229G/H226P, V229G::G225/H226P, and V229G::G225/Y252L/V253I MSDHs—In an attempt to make NADH release rate-limiting, we tried to further stabilize the adenine ring by combining new point mutations with V229G and ::G225. As mentioned above, the data obtained on ::G225 MSDH highlight the fact that mutations altering the conformation of the loop located at the entrance of the binding pocket can lead to improved stabilization of the adenine ring. To validate this assumption, a proline was introduced at position 226 in the V229G and V229G::G225 MSDHs. Substitution of a proline for His-226 mimics the molecular context of many hydrolytic ALDHs and introduces strong geometrical constraints that should modify the conformation of this loop. Therefore, we anticipated that the H226P substitution would induce a closure, even minor, of this loop on the adenine ring. On the other hand, introduction of residues with higher hydrophobic character, such as Leu and Ile, at positions 252 and 253

(α_{G} helix, supplemental Fig. S4) in V229G::G225 MSDH, would potentially increase the number of van der Waals contacts between adenine and the bottom face of the binding pocket.

The steady-state kinetic parameters determined at pH 8.2 and 30 °C are summarized in Table 2. The k_{cat} values decreased from 24- to 110-fold. More importantly, the fact that no burst of NADH production was observed under pre-steady-state conditions shows that acylation is now rate-limiting irrespective of the mutated MSDH (this result precludes comparison of the obtained K_{m} values with those determined for the wild type). As mentioned in the Introduction, the rate constant associated with the acylation step is high for the wild-type ($k_{\text{ac}} > 1000 \text{ s}^{-1}$). Therefore, the k_{ac} values are at least 1.1×10^4 - to 5×10^4 -fold lower for the mutated MSDHs. These drastic kinetic effects are likely the consequence of significant changes in the positioning of the nicotinamide ring relative to the hemithioacetal intermediate that prevent an efficient hydride transfer. Because the mutations should modify the positioning or mode of stabilization of the adenine, it is tempting to propose that changes occurring in this binding pocket can propagate to the nicotinamide ring. Although this hypothesis remains to be validated, our data clearly indicate that the cofactor binding mode is optimized in MSDH with a fine balance between the requirement for positioning of the nicotinamide ring to allow efficient hydride transfer and a degree of conformational flexibility for the deacylation to occur. Any perturbation, even minor, appears to be deleterious with respect to the efficiency of the MSDH-catalyzed reaction. The model seems to hold for the hydrolytic ALDHs. Indeed, our attempts to accelerate the rate of NADH release through "destabilization" of the adenine ring failed for retinal dehydrogenase 2 (RALDH2). The NMN moiety is known to be less stabilized in this ALDH family, at least within the ALDH/NAD(P) binary complex. Therefore, if the main anchor point (*i.e.* the adenine ring) is weakened, it is likely that the positioning of the NMN moiety within the covalent ternary complex is compromised, explaining why in the $\Delta\text{G225/G229V}$ RALDH2 acylation becomes rate-limiting with a 300-fold reduced k_{ac} (data not shown).

Conclusion—Structural dynamics associated with cofactor binding are known to play key roles in the chemical mechanism of the hydrolytic ALDHs. In this study we propose that this is also the case for their CoA-dependent counterparts. Indeed, a flip of the NMNH away from the active site is also possible in MSDH and likely the entire CoA-dependent family. This isomerization step might be required to permit nucleophilic attack of the CoA on the decarboxylated thioacylenzyme. However, in contrast to what has been established for hydrolytic ALDHs, the flip of the NMNH away from the active site leads to the complete release of NADH. Our data show that weaker stabilization of the adenine ring is a key factor in triggering the early NADH release in the MSDH-catalyzed reaction and provide for the first time structural insights into the mechanism whereby the cofactor binding mode is responsible, at least in part, for the different kinetic behaviors of the hydrolytic and CoA-dependent ALDHs. From similar three-dimensional structures, evolution has thus produced slightly different modes of cofactor binding within the ALDH superfamily. Over-

all stabilization of the cofactor results from differential contributions of both binding subsites of the cofactor; that is, mainly interactions with the adenine moiety for the hydrolytic ALDHs and the nicotinamide for the CoA-dependent ALDHs. However, in both cases the nicotinamide ring is properly positioned in the ternary complex to allow an efficient hydride transfer during the acylation step, whereas differences in the stabilization of the adenine ring lead to early or late release of the reduced cofactor.

Acknowledgments—We gratefully thank S. Boutserin for very efficient technical help and Dr. C. Stines-Chaumeil for providing the wild-type MSDH used in the crystallographic studies. We also thank Pr. K. Weissman for careful reading of the manuscript.

REFERENCES

- Marchitti, S. A., Brocker, C., Stagos, D., and Vasiliou, V. (2008) Non-P450 aldehyde oxidizing enzymes. The aldehyde dehydrogenase superfamily. *Expert Opin. Drug Metab. Toxicol.* **4**, 697–720
- Vasiliou, V., Pappa, A., and Estey, T. (2004) Role of human aldehyde dehydrogenases in endobiotic and xenobiotic metabolism. *Drug Metab. Rev.* **36**, 279–299
- Ginestier, C., Hur, M. H., Charafe-Jauffret, E., Monville, F., Dutcher, J., Brown, M., Jacquemier, J., Viens, P., Kleer, C. G., Liu, S., Schott, A., Hayes, D., Birnbaum, D., Wicha, M. S., and Dontu, G. (2007) ALDH1 is a marker of normal and malignant human mammary stem cells and a predictor of poor clinical outcome. *Cell Stem Cell* **1**, 555–567
- Huang, E. H., Hynes, M. J., Zhang, T., Ginestier, C., Dontu, G., Appelman, H., Fields, J. Z., Wicha, M. S., and Boman, B. M. (2009) Aldehyde dehydrogenase 1 is a marker for normal and malignant human colonic stem cells (SC) and tracks SC overpopulation during colon tumorigenesis. *Cancer Res.* **69**, 3382–3389
- Wang, X., and Weiner, H. (1995) Involvement of glutamate 268 in the active site of human liver mitochondrial (class 2) aldehyde dehydrogenase as probed by site-directed mutagenesis. *Biochemistry* **34**, 237–243
- Cobessi, D., Tête-Favier, F., Marchal, S., Branlant, G., and Aubry, A. (2000) Structural and biochemical investigations of the catalytic mechanism of an NADP-dependent aldehyde dehydrogenase from *Streptococcus mutans*. *J. Mol. Biol.* **300**, 141–152
- D'Ambrosio, K., Pilot, A., Talfournier, F., Didierjean, C., Benedetti, E., Aubry, A., Branlant, G., and Corbier, C. (2006) The first crystal structure of a thioacylzyme intermediate in the ALDH family. New coenzyme conformation and relevance to catalysis. *Biochemistry* **45**, 2978–2986
- Farrés, J., Wang, T. T., Cunningham, S. J., and Weiner, H. (1995) Investigation of the active site cysteine residue of rat liver mitochondrial aldehyde dehydrogenase by site-directed mutagenesis. *Biochemistry* **34**, 2592–2598
- Liu, Z. J., Sun, Y. J., Rose, J., Chung, Y. J., Hsiao, C. D., Chang, W. R., Kuo, I., Perozich, J., Lindahl, R., Hempel, J., and Wang, B. C. (1997) The first structure of an aldehyde dehydrogenase reveals novel interactions between NAD and the Rossmann fold. *Nat. Struct. Biol.* **4**, 317–326
- Muñoz-Clares, R. A., González-Segura, L., and Díaz-Sánchez, A. G. (2011) Crystallographic evidence for active-site dynamics in the hydrolytic aldehyde dehydrogenases. Implications for the deacylation step of the catalyzed reaction. *Chem. Biol. Interact.* **191**, 137–146
- Steinmetz, C. G., Xie, P., Weiner, H., and Hurley, T. D. (1997) Structure of mitochondrial aldehyde dehydrogenase. The genetic component of ethanol aversion. *Structure* **5**, 701–711
- Talfournier, F., Pilot, A., Stines-Chaumeil, C., and Branlant, G. (2009) Stabilization and conformational isomerization of the cofactor during the catalysis in hydrolytic ALDHs. *Chem. Biol. Interact.* **178**, 79–83
- Vedadi, M., and Meighen, E. (1997) Critical glutamic acid residues affecting the mechanism and nucleotide specificity of *Vibrio harveyi* aldehyde dehydrogenase. *Eur. J. Biochem.* **246**, 698–704
- Marchal, S., and Branlant, G. (1999) Evidence for the chemical activation of essential Cys-302 upon cofactor binding to nonphosphorylating glyceraldehyde-3-phosphate dehydrogenase from *Streptococcus mutans*. *Biochemistry* **38**, 12950–12958
- Rahuel-Clermont, S., Arutyunov, D., Marchal, S., Orlov, V., Muronetz, V., and Branlant, G. (2005) Thermal destabilization of non-phosphorylating glyceraldehyde-3-phosphate dehydrogenase from *Streptococcus mutans* upon phosphate binding in the active site. *J. Biol. Chem.* **280**, 18590–18597
- Cobessi, D., Tête-Favier, F., Marchal, S., Azza, S., Branlant, G., and Aubry, A. (1999) Apo and holo crystal structures of an NADP-dependent aldehyde dehydrogenase from *Streptococcus mutans*. *J. Mol. Biol.* **290**, 161–173
- Hammen, P. K., Allali-Hassani, A., Hallenga, K., Hurley, T. D., and Weiner, H. (2002) Multiple conformations of NAD and NADH when bound to human cytosolic and mitochondrial aldehyde dehydrogenase. *Biochemistry* **41**, 7156–7168
- Johansson, K., El-Ahmad, M., Ramaswamy, S., Hjelmqvist, L., Jörnvall, H., and Eklund, H. (1998) Structure of betaine aldehyde dehydrogenase at 2.1 Å resolution. *Protein Sci.* **7**, 2106–2117
- Ni, L., Sheikh, S., and Weiner, H. (1997) Involvement of glutamate 399 and lysine 192 in the mechanism of human liver mitochondrial aldehyde dehydrogenase. *J. Biol. Chem.* **272**, 18823–18826
- Pilot, A., D'Ambrosio, K., Corbier, C., Talfournier, F., and Branlant, G. (2006) Invariant Thr-244 is essential for the efficient acylation step of the non-phosphorylating glyceraldehyde-3-phosphate dehydrogenase from *Streptococcus mutans*. *Biochem. J.* **400**, 521–530
- Perez-Miller, S. J., and Hurley, T. D. (2003) Coenzyme isomerization is integral to catalysis in aldehyde dehydrogenase. *Biochemistry* **42**, 7100–7109
- Stines-Chaumeil, C., Talfournier, F., and Branlant, G. (2006) Mechanistic characterization of the MSDH (methylmalonate semialdehyde dehydrogenase) from *Bacillus subtilis*. *Biochem. J.* **395**, 107–115
- Talfournier, F., Stines-Chaumeil, C., and Branlant, G. (2011) Methylmalonate semialdehyde dehydrogenase from *Bacillus subtilis*. Substrate specificity and coenzyme A binding. *J. Biol. Chem.* **286**, 21971–21981
- Yoshida, K. I., Aoyama, D., Ishio, I., Shibayama, T., and Fujita, Y. (1997) Organization and transcription of the *myo*-inositol operon, *iol*, of *Bacillus subtilis*. *J. Bacteriol.* **179**, 4591–4598
- Goodwin, G. W., Rougraff, P. M., Davis, E. J., and Harris, R. A. (1989) Purification and characterization of methylmalonate semialdehyde dehydrogenase from rat liver. Identity to malonate semialdehyde dehydrogenase. *J. Biol. Chem.* **264**, 14965–14971
- Chambliss, K. L., Gray, R. G., Rylance, G., Pollitt, R. J., and Gibson, K. M. (2000) Molecular characterization of methylmalonate semialdehyde dehydrogenase deficiency. *J. Inher. Metab. Dis.* **23**, 497–504
- Gray, R. G., Pollitt, R. J., and Webley, J. (1987) Methylmalonic semialdehyde dehydrogenase deficiency. Demonstration of defective valine and β -alanine metabolism and reduced malonic semialdehyde dehydrogenase activity in cultured fibroblasts. *Biochem. Med. Metab. Biol.* **38**, 121–124
- Sass, J. O., Walter, M., Shield, J. P., Atherton, A. M., Garg, U., Scott, D., Woods, C. G., and Smith, L. D. (2012) 3-Hydroxyisobutyrate aciduria and mutations in the ALDH6A1 gene coding for methylmalonate semialdehyde dehydrogenase. *J. Inher. Metab. Dis.* **35**, 437–442
- Shone, C. C., and Fromm, H. J. (1981) Steady-state and pre-steady-state kinetics of coenzyme A linked aldehyde dehydrogenase from *Escherichia coli*. *Biochemistry* **20**, 7494–7501
- Söhling, B., and Gottschalk, G. (1993) Purification and characterization of a coenzyme A-dependent succinate semialdehyde dehydrogenase from *Clostridium kluyveri*. *Eur. J. Biochem.* **212**, 121–127
- Kupiecki, F. P., and Coon, M. J. (1960) Methylmalonic semialdehyde. *Biochem. Prep.* **7**, 69–71
- Dubourg, H., Stines-Chaumeil, C., Didierjean, C., Talfournier, F., Rahuel-Clermont, S., Branlant, G., and Aubry, A. (2004) Expression, purification, crystallization, and preliminary X-ray diffraction data of methylmalonate semialdehyde dehydrogenase from *Bacillus subtilis*. *Acta Crystallogr. D Biol. Crystallogr.* **60**, 1435–1437

33. Laskowski, R. A., MacArthur, M. W., Moss, D. S., and Thornton, J. M. (1993) PROCHECK: a program to check the stereochemical quality of protein structures. *J. Appl. Crystallogr.* **26**, 283–291
34. Brünger, A. T., Adams, P. D., Clore, G. M., DeLano, W. L., Gros, P., Grosse-Kunstleve, R. W., Jiang, J. S., Kuszewski, J., Nilges, M., Pannu, N. S., Read, R. J., Rice, L. M., Simonson, T., and Warren, G. L. (1998) Crystallography and NMR system. A new software suite for macromolecular structure determination. *Acta Crystallogr. D Biol. Crystallogr.* **54**, 905–921
35. Roussel, P. A., and Cambillau, C. (1991) *TURBO-FRODO, Silicon Graphics Applications Directory*, Silicon Graphics, Mountain View, CA
36. Krissinel, E., and Henrick, K. (2004) Secondary-structure matching (SSM), a new tool for fast protein structure alignment in three dimensions. *Acta Crystallogr. D Biol. Crystallogr.* **60**, 2256–2268
37. González-Segura, L., Rudiño-Piñera, E., Muñoz-Clares, R. A., and Horjales, E. (2009) The crystal structure of a ternary complex of betaine aldehyde dehydrogenase from *Pseudomonas aeruginosa* provides new insight into the reaction mechanism and shows a novel binding mode of the 2'-phosphate of NADP⁺ and a novel cation binding site. *J. Mol. Biol.* **385**, 542–557
38. Hurley, T. D., Perez-Miller, S., and Breen, H. (2001) Order and disorder in mitochondrial aldehyde dehydrogenase. *Chem. Biol. Interact.* **130**, 3–14
39. Moore, S. A., Baker, H. M., Blythe, T. J., Kitson, K. E., Kitson, T. M., and Baker, E. N. (1998) Sheep liver cytosolic aldehyde dehydrogenase. The structure reveals the basis for the retinal specificity of class 1 aldehyde dehydrogenases. *Structure* **6**, 1541–1551
40. Tsybovsky, Y., and Krupenko, S. A. (2011) Conserved catalytic residues of the ALDH1L1 aldehyde dehydrogenase domain control binding and discharging of the coenzyme. *J. Biol. Chem.* **286**, 23357–23367
41. Wallace, A. C., Laskowski, R. A., and Thornton, J. M. (1995) LIGPLOT. A program to generate schematic diagrams of protein-ligand interactions. *Protein Eng.* **8**, 127–134

SUPPLEMENTARY DATA

S1 Stereoview of NAD in MSDH from *B. subtilis*. The $2|Fo|-|Fc|$ (1σ) electron density map of NAD is shown in blue and the NAD molecule is shown in a yellow stick model.

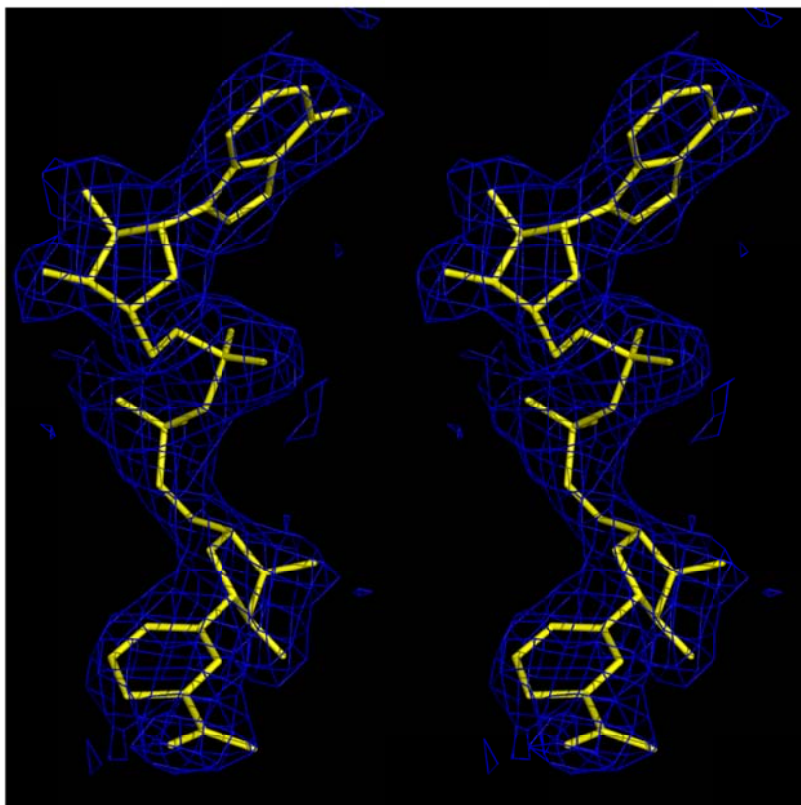
S2 Multi-sequence alignment of MSDH from *B. subtilis* and selected ALDHs: class 2 aldehyde dehydrogenase (ALDH2) from bovine liver (accession code 1ag8); retinaldehyde dehydrogenase type II (RalDH2) from Norway rat (accession code 1bi9); non-phosphorylating glyceraldehyde-3-phosphate dehydrogenase (GAPN) from *Streptococcus mutans* (accession code 1euh). Structural alignment was performed using Strap (42). The secondary structural elements of ALDH2 and MSDH are shown at the top and bottom of the alignment, respectively. The figure was prepared with ESPript.31(43).

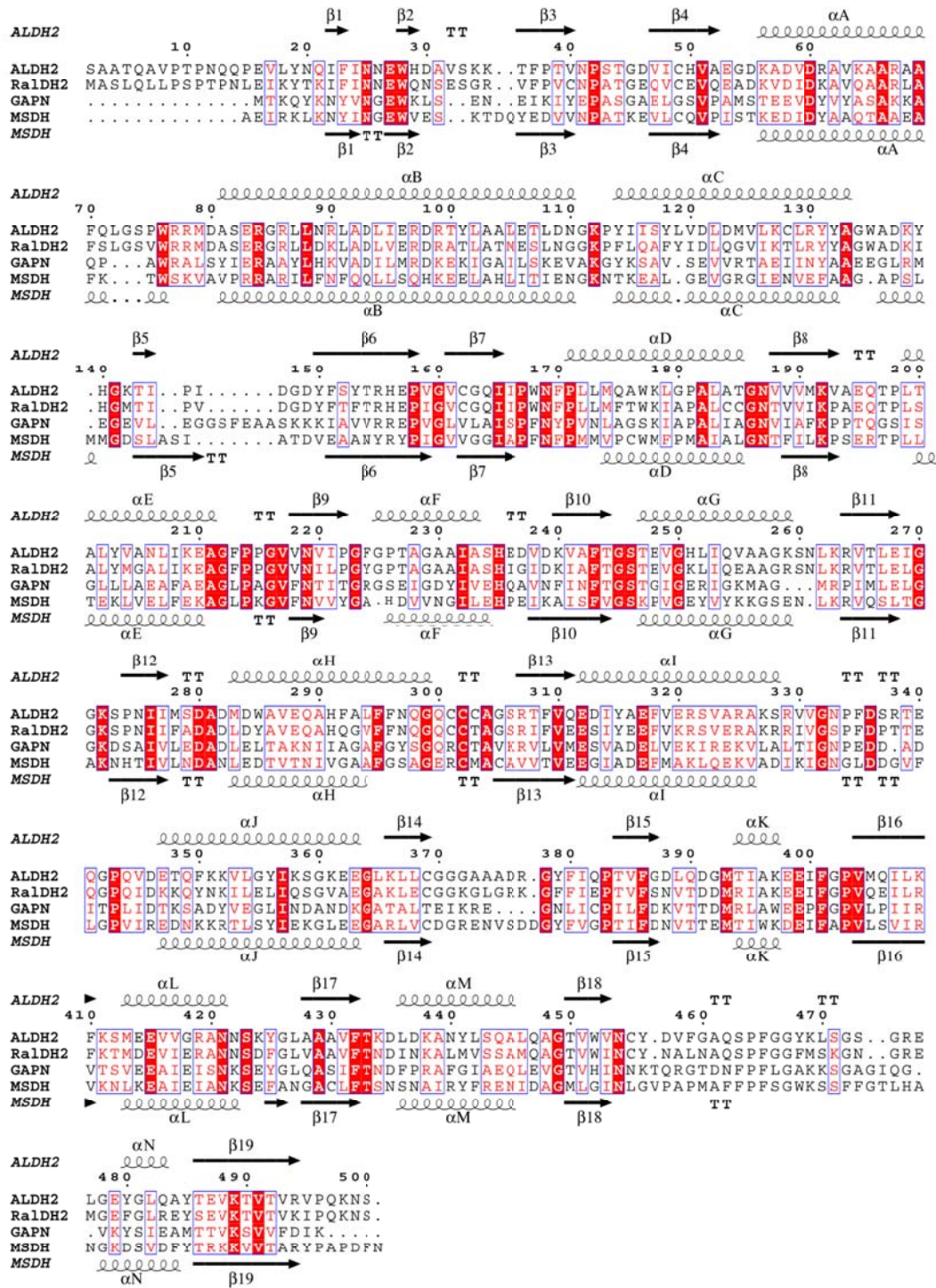
S3 Superimposition of the hydrophobic pocket postulated to act as the exit door for the reduced cofactor after isomerization. The residues from the MSDH pocket are labeled and colored by atom type. The corresponding residues from GAPN are colored yellow and are not labeled for clarity. In GAPN the pocket consists of residues Phe168, Ser246-Thr247-Gly248-Ile249, Gly270, Ile345, Asp346, Lys348, Ser349, Tyr352, Glu399-Pro400-Phe401, and Tyr425. The figure was prepared using Pymol 0.99 (www.pymol.org).

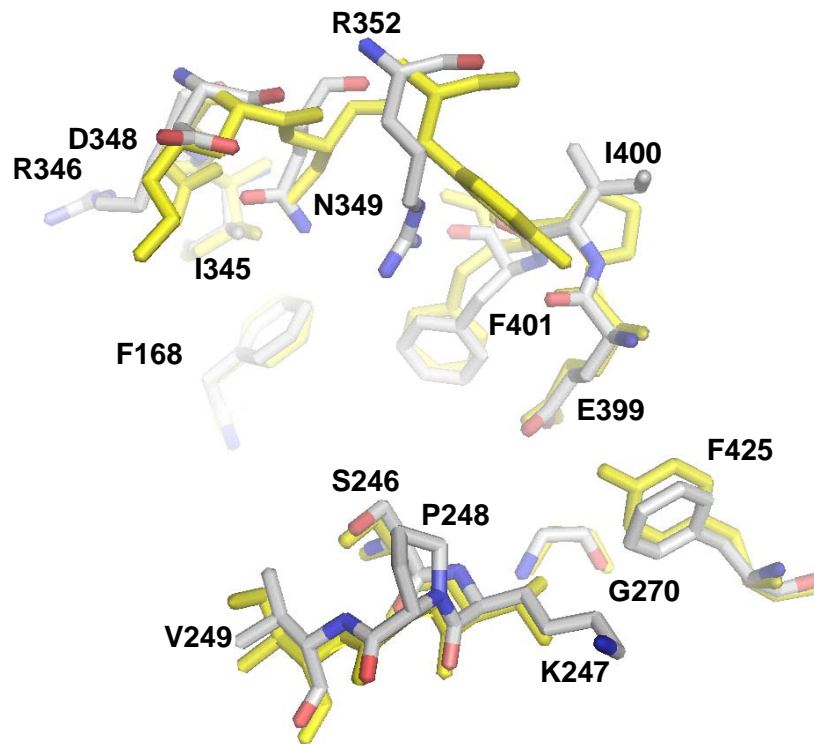
S4 The adenine binding site of (A) MSDH from *B. subtilis* and (B) rat RalDH2. The secondary structure elements contributing to the site are represented as ribbons. NAD is shown in the stick representation colored by atom type. Residues from the α_F and α_G helices that have been mutated in this study appear as sticks and are colored by atom type. The figure was prepared using Pymol 0.99 (www.pymol.org).

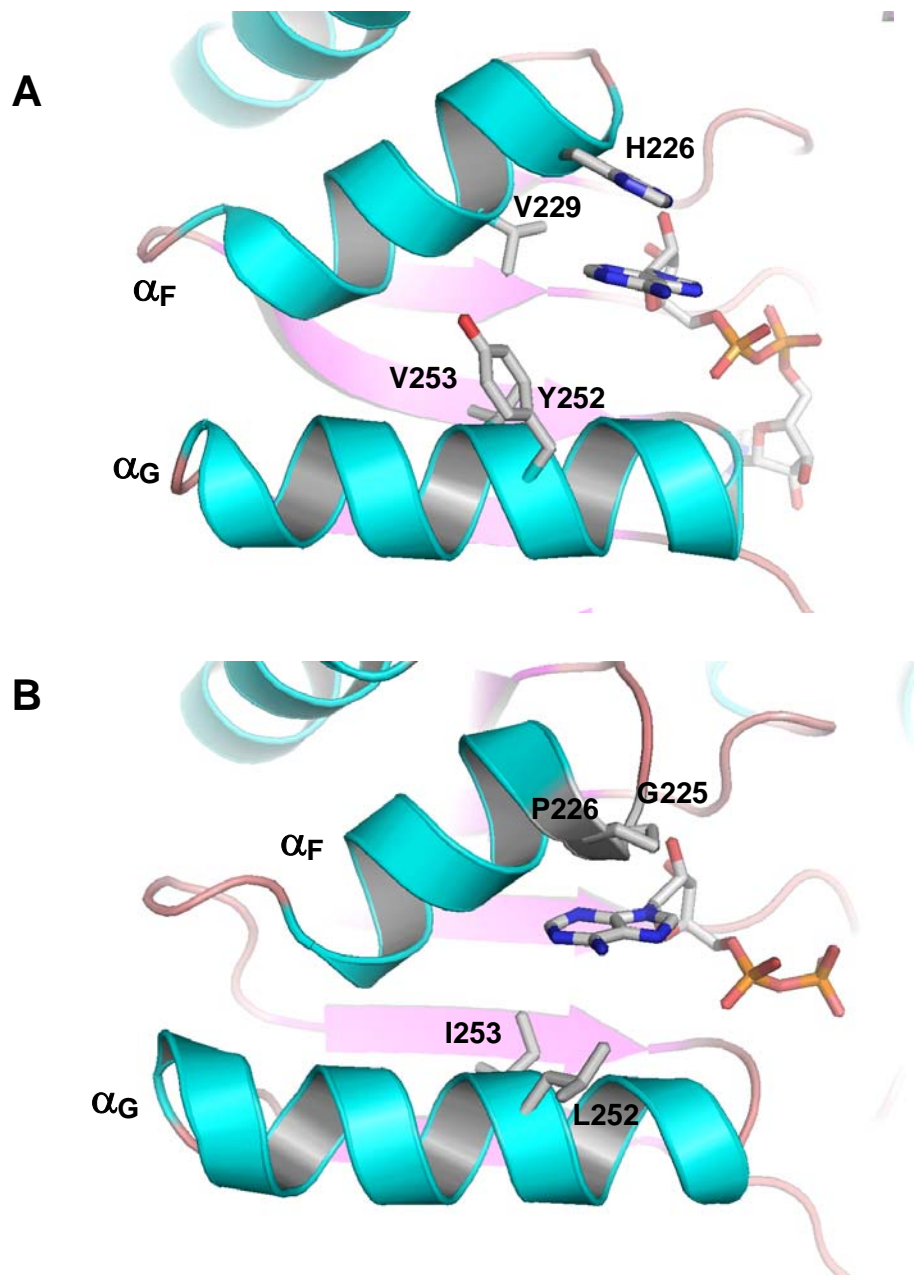
S5 Sequence alignment of the regions covering the adenine binding pocket in MSDHs and comparison with the hydrolytic human ALDH2. The sequence alignment includes MSDHs whose activity has been demonstrated (indicated by star). Sequence alignment was performed with the BioEdit software, and the numbering of amino acid residues is according to Wang and Weiner (5). The two positions shown as critical for adenine stabilization/NADH release, Val229 and the absence of Gly225, which are invariant features, are highlighted in red. Regarding the other positions studied, which are in blue, an His residue is mainly found at position 226, the hydrophobic character of the residue 253 is conserved through the presence of an isoleucine or a valine, whereas tyrosine or histidine residues are found at position 252.

S6 Representative transient for the determination of the Desulfo-CoA impact on the NADH release from the V229G::*G225* thioacylenzyme intermediate. A solution of 30 μ N 'activated'-MSDH, 30 μ N LDH (expressed in subunit) and 20 mM pyruvate was rapidly mixed at 30 °C with an equal volume of 2 mM NAD and 0.5 mM MMSA (final concentrations) in the absence (black line) or the presence (blue line) of 0.25 mM desulfo-CoA. Both syringes contained 50 mM potassium phosphate buffer, pH 8.2. The collected data were fit to a biphasic expression. The presence of desulfo-CoA led to a 2-fold decrease of the burst of NADH production and a 4-fold decrease of the amount of NADH released.









	200	210	220	230	240	250	260
<i>ALDH2 Homo sapiens</i>	TALYVANLIKEAGFPPGVVNVIPGF	GPTAGAAIASHEDVDKVAFTG	STEVGHLIQVAAGKSNLKRVT				
<i>Bacillus subtilis*</i>	LTEKLVLELFKEAGLPKGVFN	VVYGA-HDVVNGI	LEHPEIKAISFVGS	KPVGEYVYK	-GSEN	LKR	VQ
<i>Acetobacter aceti</i>	ASVMLAEIFKEAGLPDGLQV	VHGD-KDMVNAI	LEHPEIKAVS	FVGS	STPIAKH	VYAT-GTAH	GKR
<i>Pseudomonas fluorescens*</i>	STMLLVELAIEAGIPAGV	LVNVHGG-KDVVDGL	CTHKDIKAVS	FVGS	TAVGTHVYDL	-AGKH	GKR
<i>Brucella melitensis*</i>	VPMRLAELFQEAGLPAGIF	NVNGD-KESVDALL	DDPDVQAIGF	FVGS	STPIAQYI	YGR-GCANG	KR
<i>Pseudomonas aeruginosa*</i>	TSVRLAELFLEAGAPKGV	LQVVHGG-KEQVDQL	LKHPQVKAVS	FVGS	VAVGQYVYHT	-GTAHN	KR
<i>Streptomyces coelicolor*</i>	AAVKVAELLSEAGLPDGV	FNVVHGD-KVAVDR	LLEHDPKAVS	FVGS	STPIARYI	HTT-ASANG	KR
<i>Listeria innocua</i>	LMEKLVLELFSEAGLPKGV	FNVVYGA-HDVVNGI	LENETIKAVS	FVGS	KPVGEYVYKT	-GSANL	KR
<i>Listeria monocytogenes</i>	LMEKLVLELFSEAGLPKGV	FNVVYGA-HDVVNGI	LENETIKAVS	FVGS	KPVGEYVYKT	-GSANL	KR
<i>Lactobacillus rhamnosus</i>	TSQRLVLELFQEAGLPDGV	LVNVHGG-KDVVNGI	LLEHDPKAVS	FVGS	STPIAQYI	YGR-GCANG	KR
<i>Bacillus megaterium</i>	LAARLAELFEEAGLPKGV	LVNVHGG-KDVVNGI	LLEHDPKAVS	FVGS	STPIAQYI	YGR-GCANG	KR
<i>Enterococcus faecalis</i>	LMEKIVLELIEEAGF	PSGVFN	VVYGA-HDVVNT	LRLDPLVKGIS	FVGS	KNVGEYVYKE	-GTRN
<i>Sporosarcina newyorkensis</i>	LANRLAELFTEAGLPAGV	LVNVHGG-KDVVNGI	LLEHDPKAVS	FVGS	STPIAQYI	YGR-GCANG	KR
<i>Geobacillus thermoglucosid</i>	LANRLAELFTEAGLPAGV	LVNVHGG-KDVVNGI	LLEHDPKAVS	FVGS	STPIAQYI	YGR-GCANG	KR
<i>Caldalkalibacillus therman</i>	LANRLAELFQEAGLPEGV	LVNVHGG-KDVVNGI	LLEHDPKAVS	FVGS	STPIAQYI	YGR-GCANG	KR
<i>Penicillium chrysogenum</i>	AAMILAELAKEAGFPPGV	INIIHGT-APTVD	FILDEPAIKAIS	FVGS	NRAGEYI	YSR-GSANG	KR
<i>Candida albicans</i>	AAMIICELAAKAGVPAGV	LVNVHGG-KDVVNT	LRLDPLVKGIS	FVGS	KNVGEYVYKE	-GTRN	KR
<i>Aspergillus nidulans</i>	AAMILAELAREAGFPPGV	INIIHGS-AKTVD	FILDAPEIKAIS	FVGS	NRAGEYI	YTR-GSANG	KR
<i>Oryza sativa</i>	AAMMLAELAMEAGLPKGV	LVNVHGT-HDVVNNI	CDEEDIKAVS	FVGS	NIAGMHI	YSR-ASAKG	KR
<i>Populus trichocarpa</i>	ASIIILAELAMEAGLPNGV	LVNVHGT-NDIVNAI	CDDDDIRAIS	FVGS	NTAGMHI	YSR-ASAKG	KR
<i>Zea mays</i>	AAMMLAELAMEAGLPKGV	LVNVHGT-NDIVVNI	CDEEDIKAVS	FVGS	NTAGMHI	YSR-ASAAG	KR
<i>Chlamydomonas reinhardtii</i>	AAVMLADLAQQAGLPKGV	LVNVHGG-RDVVNW	I CDDPAIRAIS	FVGS	SDSAGKI	YAR-GCAAG	KR
<i>Medicago truncatula</i>	ASMLLSQLAMEAGLPEGV	LVNVHGG-HDVVNAI	CDHDDIKAIS	FVGS	SNVAGMHI	YAR-AAAKG	KR
<i>Sorghum bicolor</i>	AAMMLAELAMEAGLPKGV	LVNVHGT-NDIVVNI	CDEEDIKAVS	FVGS	NTAGMHI	YSR-ASAAG	KR
<i>Caenorhabditis elegans</i>	AAQLLVLEAKEAGVPDGC	VNIHGG-HSAVNF	ICDNPDIKAI	SFVGS	DAAGKHI	YER-GAKNG	KR
<i>Dictyostelium discoideum</i>	ASMFLVQLAQEAGVDPGV	VNVHGG-KEAVNF	ICDAPEVRAIS	FVGS	ADQAGRHI	HAR-GTANG	KR
<i>Xenopus laevis</i>	ATMLLAQLMQDAGVPDGT	LVNVHGG-HAAVNF	ICDHPAIRAIS	FVGS	SNQAGEYI	YER-GSRNG	KR
<i>Danio rerio</i>	CTMMLAKLLQDAGAPDGT	LVNVHGG-HDAVNF	ICDHPAIRAIS	FVGS	SNQAGEYI	YER-GSKNG	KR
<i>Drosophila melanogaster</i>	ATMLLMELLNEAGCPPGV	VNVHGG-HDAVNF	ICDAPEIKAVS	FVGS	DQAGKI	YER-AGKNG	KR
<i>Gallus gallus</i>	ALMFLAKLFQDAGAPDGT	LVNVHGG-HEAVNF	ICDHPDIRAIS	FVGS	SNQAGEYI	YER-GSRNG	KR
<i>Rattus norvegicus*</i>	ATMLLAKLLQDAGAPDGT	LVNVHGG-HEAVNF	ICDHPDIRAIS	FVGS	SNQAGEYI	YER-GSRNG	KR
<i>Bos taurus</i>	ATMLLAKLFQDAGAPDGT	LVNVHGG-HEAVNF	ICDHPDIRAIS	FVGS	SNQAGEYI	YER-GSRHG	KR
<i>Homo sapiens*</i>	ATMLLAKLLQDAGAPDGT	LVNVHGG-HEAVNF	ICDHPDIRAIS	FVGS	SNKAGEYI	YER-GSRHG	KR

